Towards in-cell structural study of light-harvesting complexes : an investigation with MAS-NMR

Azadi Chegeni, F.

CHAPTER 5

In-vivo NMR as a tool for probing molecular structure and dynamics in intact *Chlamydomonas reinhardtii* cells

This work is published as: Azadi-Chegeni F., Schiphorst C. & Pandit A.
Photosynthesis research (2018), 135(1-3): 227-237

Abstract

We report the application of NMR dynamic spectral editing for probing the structure and dynamics of molecular constituents in fresh, intact cells and in freshly prepared thylakoid membranes of *Chlamydomonas reinhardtii* (*Cr*.) green algae. For isotope labeling, wild type *Cr*. cells were grown on ^{13}C acetate-enriched minimal medium. 1D ^{13}C *J*-coupling based and dipolar-based MAS NMR spectra were applied to distinguish ^{13}C resonances of different molecular components. 1D spectra were recorded over a physiological temperature range and whole-cell spectra were compared to those taken from thylakoid membranes, evaluating their composition and dynamics. A theoretical model for NMR polarization transfer was used to simulate the relative intensities of direct, *J*-coupling and dipolar-based polarization from which the degree of lipid segmental order and rotational dynamics of the lipid acyl chains were estimated. We observe that thylakoid lipid signals dominate the lipid spectral profile of whole algae cells, demonstrating that with our novel method, thylakoid membrane characteristics can be detected with atomistic precision inside intact photosynthetic cells. The experimental procedure is rapid and applicable to fresh cell cultures, and could be used as an original approach for detecting chemical profiles, and molecular structure and dynamics of photosynthetic membranes *in vivo* in functional states.

Introduction

The plasticity of oxygenic photosynthetic membranes is tightly connected with plant fitness in fluctuating environments and their capability to respond to stress in excess light or drought conditions. Regulation of photosynthetic light harvesting is controlled by flexibility of the light-harvesting antenna from atomistic to supra molecular scale. Short and long-term adaptation results in structural, dynamical changes varying from atomic-scale pigment and protein alterations to mesoscopic membrane rearrangements [1-4]. Fast membrane remodeling is required to cope with sunlight fluctuations, while photosynthetic organisms may adjust their membrane compositions in adaptation to varying seasons or climates. The underlying regulation mechanisms have to be understood to the molecular level to gather central knowledge that can be used to increase plant stress tolerance or design algae species with improved solar-to-biomass conversion.

Essential here is the parallel development of suitable tools and methodology that can analyze molecular composition, structure and plasticity of intact photosynthetic membranes of plants and cells grown under various environmental conditions or in different functional states. Fluorescence techniques have been developed for functional analysis of whole membranes, cells, or leaves, probing the dynamic nature of light harvesting *in vivo* in molecular detail [5-8]. Complementary techniques that can resolve conformational structures and dynamics at the molecular level inside physiological membranes or whole cells are still challenging. With Fourier-Transform Infra-Red (FTIR) spectroscopy, molecular information of protein carbonyls and lipids can be obtained from heterogeneous membranes, but has to be extracted from band fitting of broad FTIR absorbance spectra. The technique has been applied to determine the dynamics of protein and lipid moieties in *Synechocystis* cells and in higher-plant thylakoid membranes [9-10]. Resonance Raman (RR) spectroscopy can report on the conformations and H-bonding patterns of chromophores in intact systems and through this technique, it was discovered that light stress induces *in-vivo* and *in-vitro* changes in the conformation of neoxanthin (Neo) [11]. Fluorescence Recovery After Photobleaching (FRAP) was used to investigate the lateral mobility of light-harvesting complexes in cyanobacteria and in plant thylakoid membranes [12]. Thylakoid membrane fluidity has been investigated by measuring the rotational dynamics of externally added fluorescence or Electron Spin Resonance (ESR) spin probes [4]. The latter techniques, however, do not report on the intrinsic, molecular dynamics of the membrane components. ^{31}P NMR and fluorescence studies using fluorolipid probes have been applied to detect mesoscopic phase transitions in functional thylakoid membranes, and detected a transition from bilayer to inverted hexagonal states at high temperature [13-14]. The advantage of ^{31}P NMR is that no external probes are added and no isotope enrichment is required, the disadvantage is however that only the phases of the phospholipids are followed, which in thylakoids only form ~10% of the total lipid composition. Recent multi-scale modeling simulations have provided molecular insight in thylakoid lipid lateral organization and dynamics [15] and predicted the molecular dynamics of Photosystem II embedded in a thylakoid membrane [16-17]. These studies have not been matched by experimental approaches, which would require detection of protein and lipid dynamics with atomistic resolution in native thylakoids, or atomic-level structural analysis of isolated pigment-protein complexes reconstituted in thylakoid lipid membranes.

Herein we describe the use of dynamic spectral-editing NMR as a new tool to analyze molecular composition and dynamics of thylakoid membranes or whole cells. Arnold et al. demonstrated that lipid and saccharide constituents could be identified in whole microalgae cells using NMR dynamic spectral-editing to

improve spectral resolution [18]. Topgaard and Sparr developed polarization transfer solid-state NMR into a method that allowed them to detect molecular mobility in intact skin [19] and to determine surfactant phase transitions [20]. In chapter 2, we elaborated on these approaches to separate rigid and mobile thylakoid constituents in *Chlamydomonas reinhardtii* (*Cr*.) thylakoids [21] and demonstrated that protein and lipid molecules in zeaxanthin (Zea)-accumulating *npq2* thylakoids display differential dynamics compared to WT (CW15) membranes, providing a molecular explanation for reported increased rigidity in Zea-rich membranes.

In this chapter, we demonstrate that our approach can be applied directly to fresh *Cr*. cells, circumventing isolation procedures and the need for sample storage. By simulating the polarization transfer efficiencies, we show that lipid acyl-chain rotational dynamics and their degree of segmental order can be estimated within a certain range, in a quantitative way. Comparison of intact *Cr*. cells and freshly isolated thylakoid membranes show very similar NMR lipid spectral profiles, demonstrating that the thylakoid lipids dominate and implying that their molecular conformation and dynamics can be determined inside intact cells.

Material & Methods

Cell culturing and ^{13}C isotope labeling

Wild-type *Cr*. cells (*strain* CC-124) were grown mixotrophically on Tris-Acetate-Phosphate (TAP) medium in a home-built set up, under continuous illumination with cool white LEDs (~50 μmol/m^2 s) and constant temperature of 25^{o}C. For isotope-label incorporation, the acetic acid was replaced by ^{13}C- acetate (Cambridge Isotopes).

Pigment analysis

Chlorophyll and carotenoid concentrations were determined based on [22], using a home-written Javascript web application that performs a non-negative least-square fitting procedure based on Lawson and Hanson [23] and Bro and de Jong [24]. In addition, pigment extracts were analyzed by High-Performance Liquid Chromatography (HPLC).

Thylakoid extraction

The isolation of thylakoids was performed according to Chua and Bennoun [25] with some modifications. Cells were harvested in the exponential growth phase, centrifuged and resuspended in 0.2 volumes of $MgCl_2$ buffer (1mM $MgCl_2$, 0.1 M HEPES, pH 7.5/KOH, 10% sucrose). Cells were ruptured by sonication on a 2500 Watt sonicator at 10%, using 15 cycles of 1s on/10s off followed by 30 cycles of 2s on/10s off. Thylakoid membranes were isolated using a discontinuous sucrose gradient. The disrupted cells were overlaid with 3mL of 1.8M sucrose in EDTA buffer, 1ml of 1.3M sucrose EDTA buffer, 1 ml of 0.5M sucrose EDTA buffer and 5ml of EDTA buffer without sucrose. The gradients were ultra-centrifuged for one hour at 4 ^{o}C in a SW41 swing rotor (Beckmann) at 24000 rpm (100000×g).

Solid-state NMR

NMR spectra were recorded with a Bruker Advance-III 750 MHz wide bore NMR spectrometer. NMR samples were prepared by mild centrifugation of fresh cell or thylakoid suspensions into a 4mm NMR rotor that was used with a top insert. For cell samples, approximately 50mL of cell culture was used and concentrated into the rotor, from which we estimate that samples contained about 0.5mg of Chl. Magic Angle Spinning was performed at 5 kHz for whole cells and at 13 kHz for thylakoid extractions. Cross polarization (CP) experiments were performed with a 2ms CP contact time (τ_{CP}), 5s recycle delay and 20ms acquisition time, $\omega_1^C/2\pi$ of 40.3 kHz and ^{1}H nutation frequency linearly ramped from 80 to 100 kHz. Insensitive Nucleus Enhanced Polarization Transfer (INEPT) experiments were performed with two delays of 1.25ms and an acquisition time of 80ms. For direct polarization (DP) experiments, the delay was set at 5s and the acquisition time was set to 43ms. The dead time after pulse excitation before acquisition was 4.5 microseconds. Data were processed and analyzed in TopSpin3.2 and MNova. Temperature were calibrated analyzing ^{207}Pb NMR chemical shifts of lead nitrate ($Pb(No_3)2$) [26].

Simulation of INEPT and CP intensities

CP and INEPT intensities relative to DP as function of rotational correlation time τ_c and order parameter S were estimated by using the following equations taken from [27-28]:

$$\frac{I_{\mathrm{CP}}}{I_{\mathrm{DP}}} = \frac{\gamma_{\mathrm{H}}}{\gamma_{\mathrm{C}}} \frac{\exp\left(-\frac{\tau_{\mathrm{CP}}}{T_{1\rho}^{\mathrm{H}}}\right) - \exp\left(-\frac{\tau_{\mathrm{CP}}}{T_{\mathrm{CH}}}\right)}{1 - \frac{\tau_{\mathrm{CH}}}{T_{1\rho}^{H}}}, \quad (1)$$

in which the gyromagnetic ratios of ^{1}H and ^{13}C are equivalent to 267.5 (10^6 rad S^{-1} T^{-1}) and 67.2 (10^6 rad S^{-1} T^{-1}), respectively, $T_{1\rho}^{\mathrm{H}}$ is the ^{1}H spin-lattice relaxation time in the rotating frame, T_{CH} is the time constant for cross-polarization and τ_{CP} is the contact time for cross polarization.

$$\frac{I_{\mathrm{INEPT}}}{I_{\mathrm{DP}}} = \frac{\gamma_{\mathrm{H}}}{\gamma_{\mathrm{C}}} n \sin(2\pi J_{\mathrm{CH}}\tau) \sin(2\pi J_{\mathrm{CH}}\tau') \, cos^{n-1}(2\pi J_{\mathrm{CH}}\tau') \exp\left(-\frac{2\tau}{T_2^{\mathrm{H}}} - \frac{2\tau'}{T_2^{C}}\right), \quad (2)$$

in which n is the bond multiplicity, J_{CH} is the ^{1}H-^{13}C through bond scalar coupling constant, and T_2^{H} and T_2^{C} are the effective ^{1}H and ^{13}C transverse dephasing times. The DP intensities in the equation are the theoretical intensities assuming that total polarization relaxation occurs after each pulse. The coherence evolution times τ=1/4J_{CH} and τ' =1/6J_{CH} are delays between the radio frequency (rf) pulses in the INEPT sequence. T_2^{H}, T_2^{C}, $T_{1\rho}^{\mathrm{H}}$ and T_{CH} values were estimated from a rotational correlation function that describes time-averaged fluctuations of the local magnetic field due to chemical-bond vector reorientations, depending on τ_c and S (see [20] and [28]). Experimental parameters that were used as input for the simulations were τ_{CP}=2ms, J_{CH}=133.3 Hz, $\omega_1^{\mathrm{C}}/2\pi$=86 kHz, $\omega_1^{\mathrm{C}}/2\pi$=40.3 kHz, $\omega_0^{\mathrm{C}}/2\pi$=86 MHz, $\omega_0^{\mathrm{H}}/2\pi$= 188 MHz, τ_{S}=1 ms, ω_{R}=5 kHz for cells and 13 kHz for isolated thylakoid membranes. Curves of the relative INEPT intensities as function of rotational correlation time τ_C and order parameter S were generated using MathCad 15.0.

Results and Discussion

Spectral editing and assignment of molecular constituents in *Cr.* intact cells

Figure 1A presents a DP, CP and INEPT ^{13}C spectrum of *Cr.* cells. We performed an assignment of the most prominent peaks in the ^{13}C spectra. Most of the assignments are based on the following references and are summarized in table 1 [18, 29-32]. Many assignments are ambiguous and peaks correspond with reported NMR resonances of more than one possible carbon atom type, as indicated. *Cr.* lipid composition consists of monogalactosyldiacylglycerol (MGDG), digalactosyldiacylglycerol (DGDG), sulfoquinovosyldiacylglycerol (SQDG), diacylglyceryltrimethylhomo-Ser (DGTS), phosphatidylglycerol (PG) and phosphatidylethanolamine (PE) in descending order of abundance, and in case of overlapping peaks we only specify fatty acid (FA) chain length and degree

of unsaturation, based on [30]. The region 10-40 ppm contains the protein side chain resonances that accumulate in a broad peak, together with the lipid FA CH_2 and CH_3 signals, which are the sharp peaks superimposed. The protein C_α signals are visible between 50-70 ppm and partly overlap with carbohydrate signals that are visible in the region 70-100 ppm. The region 125-135 ppm contains the signals of the aromatic protein side chains and double-bonded CH signals of the lipid FA. The protein backbone carbonyl signals accumulate between 170-180 ppm. Chl and xanthophyll signals are relative weak and coincide with other peaks. Figure 1 presents DP, CP and INEPT ^{13}C spectra of *Cr.* whole cells (1A) and of thylakoid membranes (1B) and in figure 2 the spectrum of thylakoids and those of whole cells are superimposed for each type of NMR experiment. The lipid patterns in the aliphatic region (10-40 ppm) and aromatic region (125-135 ppm) are remarkably similar for both types of samples, which indicates that in whole cells, most of the lipids belong to the thylakoids. As expected, the signals from cell-wall components, starch or DGTS are absent in the spectra of thylakoids. The thylakoid membranes were purified with sucrose gradients, and signals in the region 70-100 ppm could originate from galactosyl lipid head groups but also from natural-abundant ^{13}C of the sucrose present in the buffer. Between 135-140 ppm a weak shoulder of the xanthophylls becomes visible in the DP and CP spectra of thylakoids. The protein carbonyl band has more intensity in the CP spectrum of thylakoids than in whole cells. This is because thylakoids contain membrane proteins that are relatively rigid and enhanced in CP, whereas intact cells contain a mixture of membrane and soluble proteins with higher mobility. The CH peaks of the unsaturated CH_3 fatty acids (FA) have much higher intensities in INEPT than in CP and the 132 ppm peak of the C16 carbons towards the FA end-tail are absent in CP, indicating that the majority of the CH_3 FA chains have low segmental ordering and highly dynamic FA tails.

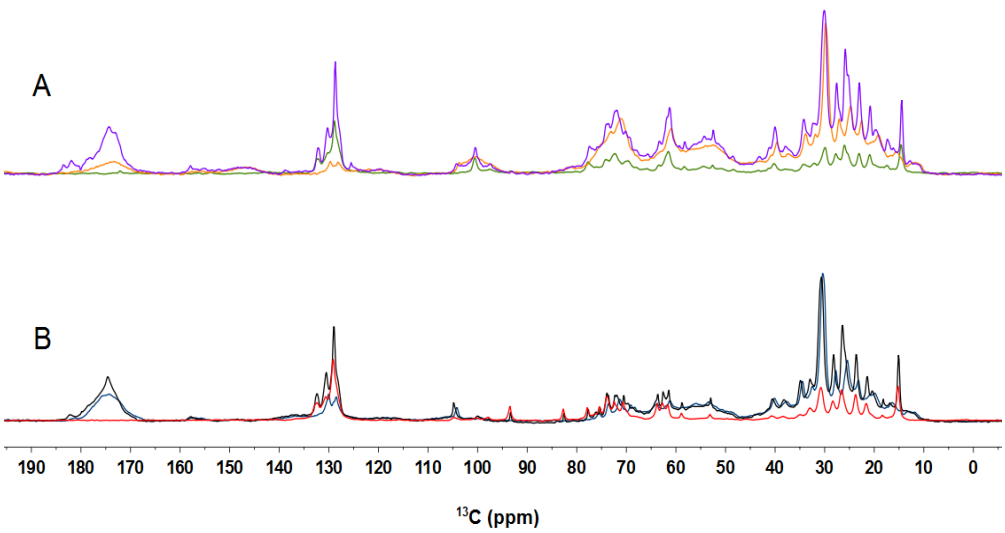

Figure 1. A: Overlaid ^{13}C-DP (purple), ^{13}C -CP (orange) and ^{13}C-INEPT (green) spectra of whole cells recorded at 13.5 °C. **B:** Overlaid ^{13}C-DP (black), ^{13}C -CP (blue) and ^{13}C-INEPT (red) spectra of isolated thylakoids recorded at 13.5 °C.

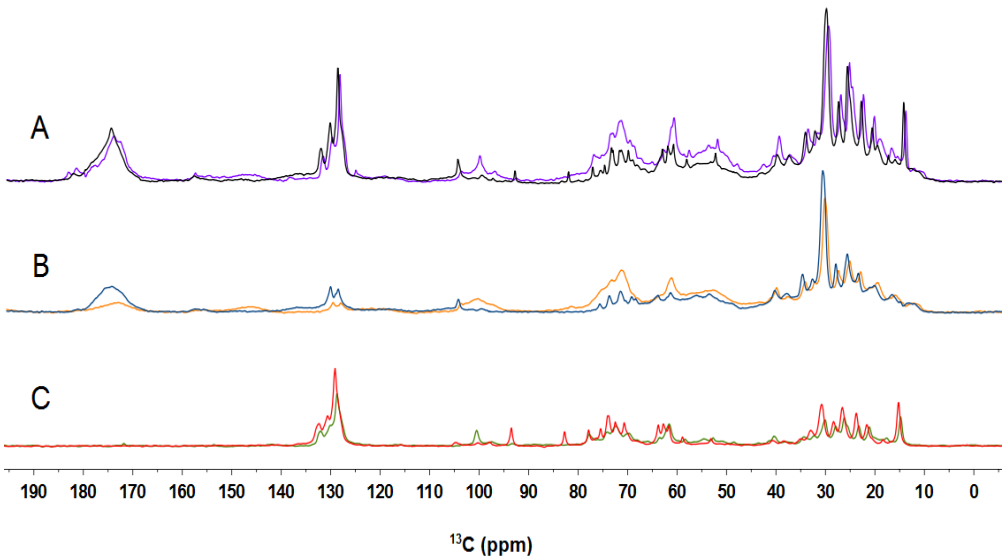

Figure 2. Overlaid DP, CP and INEPT spectra of whole cells and thylakoids recorded at 13.5^{0}C. **A:** DP spectra of whole cells (purple) and thylakoids (black). **B:** CP spectra of whole cells (orange) and thylakoids (blue). **C:** INEPT spectra of whole cells (green) and thylakoids (red).

Chemical shift (ppm)	Assignment	INEPT	CP	Reference
12.6	Ile $C_{\delta 1}$; xanth 9/13-Me		×	31, 33
14.6	lipid CH_3	×		30, 34
21.0	lipid (*ω–1)* CH_2 18:3	×	×	30
23.2	Lipid (*ω-1)* CH_2 16:1/16:0	×	×	30
26.0	lipid C3	×	×	30,18
27.8	lipid C8 18:3	×	×	30
30.2	lipid nCH_2	×	×	34
32.5	lipid C14 16:1/16:0	×	×	30
34.5	lipid C2; Lut/Neo C1	×	×	30, 31
37.6	Chl P7/11 phy; glycoprotein C3; xanth C1	×	×	32, 31
40.1	Chl phytols P8/10/12; xanth C4	×	×	32, 31
52.6	glycoprotein C; PC C_γ	×	×	18
61.7	Glyc C1/C3; glycoprotein C2	×	×	18, 34
63.5	Glyc C1/C3	×		18, 34
71.5	MGDG G3		×	18, 34
72.5	lipid G2/3/5, starch C2/5	×		18
73.6	lipid G2/3		×	18, 34
74.3	starch C3	×	×	18
78.0	glycoprotein C4	×		18
98.0	SQDG/DGDG G1	×	×	18, 34
100.5	DGDG G1, starch C1	×	×	18
104.2	MGDG G1; cell wall C1	×	×	18, 34
128.6	lipid C10 18:3	×	×	30
130.1	lipid C9/12/13 18:3	×	×	30, 31
132.0	lipid C16 18:3	×		30, 31
157.7	Arg C_ζ			33
171.9	lipid C1/CO	×		18
172.6	DGTS C1/CO			18
174.2	PG C1			18
181.7	Glu/Asp COO^-		×	33
183.1	Glu/Asp COO^-		×	33

Table 1. Chemical shift assignments. Crosses indicate that the peak is observed in the ^{13}C INEPT, resp. CP spectrum. Xanth: xanthophyll; Phy: Chl phytol chain; Lut: lutein; Neo: neoxanthin; Glyc: glycerol.

Temperature dependence

The dynamic behavior of protein and lipid components was further explored by varying the temperature in a physiological range. For thylakoid membranes, the temperature was not raised above 23.3 °C to make sure that no irreversible damage would occur. For whole cells, the temperature was raised to 37.8 °C. To check if heating caused irreversible changes, the temperature was raised and lowered again after which samples were re-measured, verifying that no heating-induced changes had taken place (*data not shown*). We noticed a decrease of

signal intensity in DP spectra over time, which could be caused by the effect of magic-angle spinning, slowly sedimenting the cells at the rotor walls and changing the filling factor. To correct for time-dependent intensity changes, the CP and INEPT intensities were divided by the DP intensities of the respective peaks. Figure 3 presents the temperature-dependent CP over DP and INEPT over DP signal intensities of whole-cell spectral components and figure 4 presents the temperature curves obtained from thylakoid spectra. The intensities are normalized with respect to the intensity at 3 °C for better comparison. The thylakoid INEPT-observed components (4C) show an increase with temperature that seems to stabilize for around 20 °C for the CH and FA end-tail carbons. The thylakoid CP-observed components (4A, B) show a decrease of CP efficiencies with temperature except for the $n\mathrm{CH_2}$ carbons. Because INEPT signals are sensitive for highly mobile components and CP signals are enhanced for more rigid molecules, this behavior is in line with expected increase of mobility at higher temperatures. The whole-cell CP-observed components (3A, B) also show an overall decrease of CP efficiencies with temperature, but unexpectedly the INEPT-observed intensities (4C, D) only increase up to 13.5°C and stabilize or decrease at higher temperatures, suggesting that their dynamics is reduced.

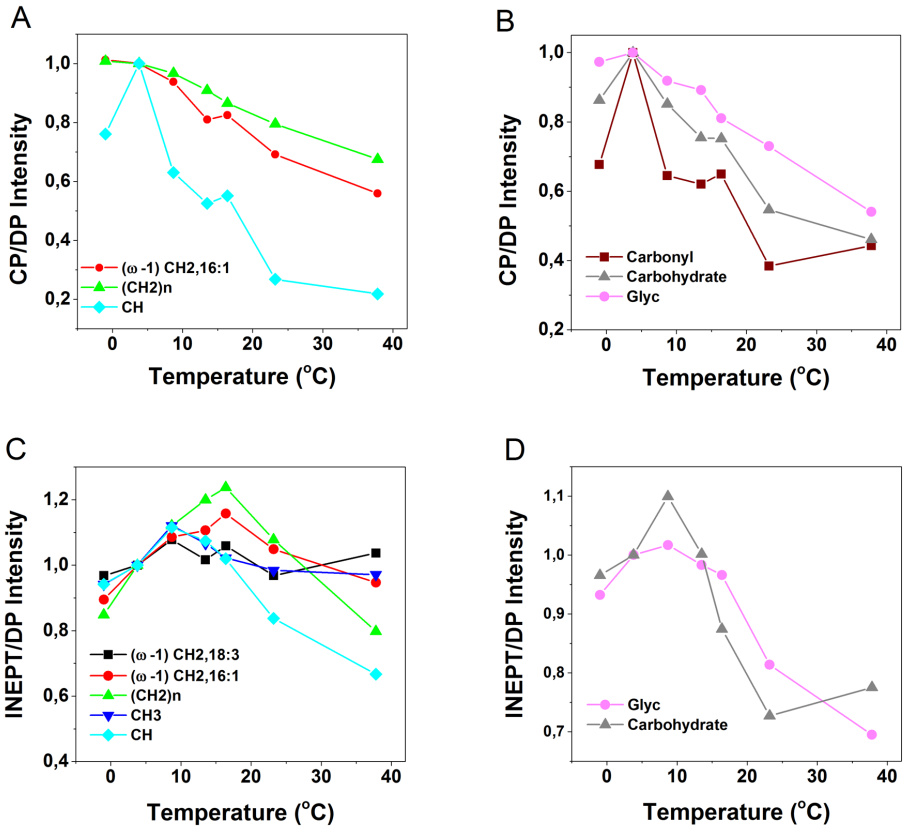

Figure 3. ^{13}C CP and INEPT intensities of whole-cell components as a function of temperature. The intensities are normalized at T=3 °C. **A:** CP intensities of fatty acids. Red circles: (ω-1) CH_2 of 16:1; green triangles: nCH_2; light-blue squares: CH. **B:** CP intensities of protein carbonyls and carbohydrates. Dark-red squares: carbonyl; gray triangles: galactosyl and glycerol carbons (Galac) of glycerolipids; pink circles: glycoprotein and glycerol C1/C3 carbons (Glyc). **C:** INEPT intensities of fatty acids. Black squares: (ω-1) CH_2 of 18:3; red circles: (ω-1) CH_2 of 16:1; green triangles: nCH_2; dark blue triangles: CH_3; light blue squares: CH. **D:** INEPT intensities of protein carbonyls and carbohydrates. Grey triangles: galactosyl and glycerol carbons of glycerolipids; pink circles: glycoprotein and glycerol C1/C3 carbons

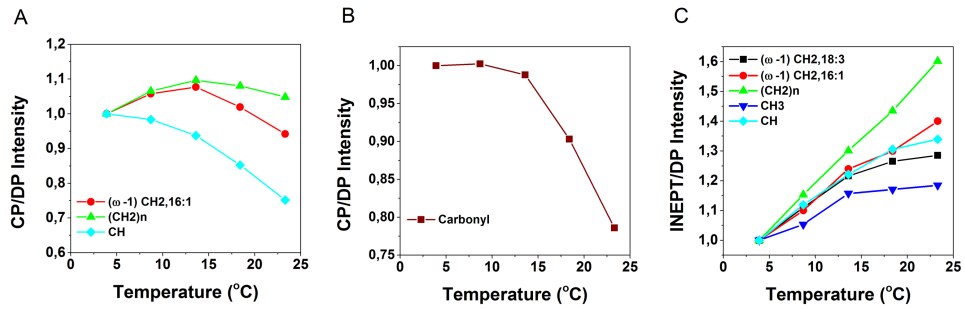

Figure 4: ^{13}C CP-MAS and INEPT intensities of thylakoids as a function of temperature. **A:** CP intensities of fatty acids. Red circles: (ω-1) CH_2 of 16:1; green triangles: $n CH_2$; light-blue squares: CH. **B:** CP intensities of protein carbonyls. **C:** INEPT intensities of fatty acids. Black squares: (ω-1) CH_2 of 18:3; red circles: (ω-1) CH_2 of 16:1; green triangles: CH_2; dark-blue triangles: CH_3; light-blue squares: CH.

Simulated INEPT and CP efficiencies

To gain more insight how the experimentally obtained INEPT and CP intensities related to molecular dynamics and segmental ordering, we simulated the INEPT and CP intensities as function of rotational correlation time τ_C and order parameter S, using our experimental NMR parameters as input. In figure 5, we show the theoretical INEPT polarization transfer efficiency for a CH segment. Figure 5A and B present I_{INEPT}/I_{DP} as a function of correlation time (τ_C) and of order parameter (S) at MAS frequency of 13 kHz (simulating the thylakoid experiment), and 5C and D present I_{INEPT}/I_{DP} calculated for a MAS frequency of 5 kHz (simulating the whole-cell experiment). At both MAS frequencies, INEPT starts to be effective for correlation times below 0.1 µs (τ_C <0.1 µs) and approaches a maximum (I_{max}) at τ_C <1 ns. In the sub-nanosecond dynamics range, the INEPT intensities only depend on the segmental order parameter S. At 13 kHz MAS, INEPT becomes effective at $S < 0.2$, while at 5 kHZ, INEPT becomes effective at $S < 0.05$, and has a lower I_{max}. We performed the same analysis for CH_2 and CH_3 segments and summarized the results in table 2.

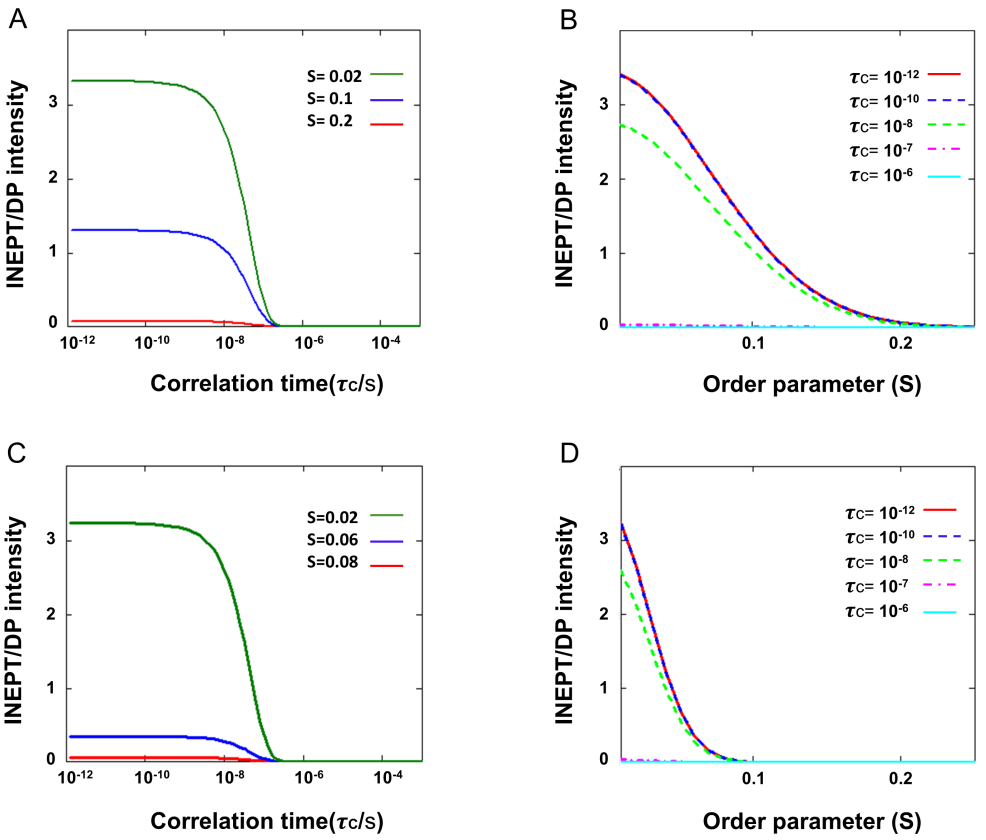

Figure 5. Simulated INEPT/DP intensities as a function of order parameter S and rotational correlation time τ_C for a CH segment. **A**: INEPT/DP intensities for ω_R=13 kHz as function of τ_C at S=0.2, 0.1 and 0.02. **B**: INEPT/DP intensities for ω_R=13 kHz as a function of S at τ_C=10^{-12}, 10^{-10}, 10^{-8}, 10^{-7} and 10^{-6} seconds. **C**: INEPT/DP intensities for ω_R=5 kHz as a function of τ_C at S=0.08, 0.06 and 0.02. **D**: INEPT/DP intensities for ω_R=5 kHz as a function of S at τ_C=10^{-12}, 10^{-10}, 10^{-8}, 10^{-7} and 10^{-6} seconds.

Spinning frequency (ω_R)		Correlation time (τ_c)	Order parameter (S)
5kHz	CH	<0.1 µs	<0.08
	CH_2	<0.05 µs	<0.05
	CH_3	<0.05 µs	<0.1
13kHz	CH	<0.1 µs	<0.2
	CH_2	<0.05 µs	<0.1
	CH_3	<0.05 µs	<0.03

Table 2. Theoretical conditions for observing INEPT intensities at 5 kHz (simulating the whole-cell experiments) and 13 kHz (simulating the thylakoid experiments

Figure 6 presents the theoretical I_{CP}/I_{DP} intensities as a function of correlation time for a CH segment. The predicted CP intensities were identical for 5 kHz and 13 kHz. Figure 6 shows that CP is effective for correlation times between nanoseconds and seconds, except for a gap in the microsecond range in which CP gives no signal. The same behavior as function of the correlation time is observed for different order parameter values (S=0.05, 0.1 and 0.5) except that for $S \geq 0.5$, CP has non-zero intensity for sub-nanosecond τ_C values. Hence, CP is effective for oriented molecules with restricted motions, even if they exhibit very fast dynamics.

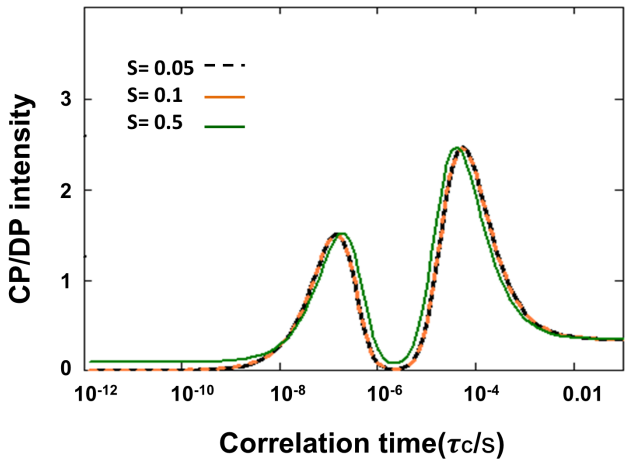

Figure 6. Simulated CP/DP intensities as a function of rotational correlation time τ_C for S = 0.05, 0.1 and 0.5.

Dynamics of *Cr.* cell and thylakoid molecular components

We used the simulations to estimate the dynamics of *Cr.* cell constituents, in particular of the lipids, of which signals are observed both in INEPT and CP. The simulated intensity ratios use I_{DP} assuming that DP is effective over the whole frequency range. The experimentally observed DP intensities however depend on $T1$ and on the delay time t_d between scans, so that $I_{DP}/I_{DP\ theory} = 1\text{-}\exp(-t_d/T_1^C)$. With our experimental settings we assume that DP intensities are attenuated for components with $\tau_C > 1\mu s$. Since the DP spectra show significant intensity for most of the cell and thylakoid components, we presume that these have dynamics in the sub-microsecond range. Comparing the spectral profiles of whole-cells and thylakoids (figure 2), we conclude that the whole-cell INEPT spectrum is dominated by the signals of the thylakoid lipids. The higher intensities observed for the thylakoid INEPT spectrum compared to the whole-cell INEPT spectrum, relative to the DP intensities (figure 1A an B) can be explained by the increased MAS frequency used for the thylakoid experiments that renders INEPT more efficient, as illustrated in the model. The largest nCH$_2$ lipid peak at 30 ppm has similar intensity in CP and DP for both whole cells and thylakoids (figure1A and B), conforming to $I_{CP/DP} \sim 1$ in our model. Focusing on the sub-microsecond regime where DP is effective, $I_{CP/DP} \sim 1$ matches with τ_c*'s* in the order of 50 ns. In contrast to the nCH$_2$ carbons, the CH carbons have much larger signals in INEPT than in CP, implying that they have conformational dynamics with $\tau_c < 10$ ns and a large degree of disorder ($S < 0.05$ for whole cells). The lipid CH carbons are the bended, lower part of the unsaturated FA chains, while the nCH$_2$ FA carbons are located toward the lipid head groups. The lipid FA chains of the unsaturated lipids thus become more dynamic towards the end tails, which are disordered and undergo fast motions.

In the temperature profiles of the intact cells (figure 3), we observe overall a decay of the CP intensities for lipid (3A), and protein backbone and cell wall (3B) components at higher temperatures, indicating that the cell components have increased molecular motions. The lowest temperature point in the curves in figure 3 was close to zero Celsius, which could have led to non-linear temperature effects, and might explain the observed increase instead of decrease of CP signal between the two lowest temperature points. The INEPT-observed lipid signals (3C) increase for temperatures up to ~13 ^{o}C, indicating that the lipid segments increase their conformational dynamics, or become more disordered. Above this temperature, the signals remain constant for the end-tail carbons, suggesting that their conformational dynamics enter the sub-nanosecond regime where INEPT becomes insensitive to further changes in dynamics, and that there is no change in lipid disorder. Interestingly, the INEPT-observed nCH$_2$, CH (3C) and galactosyl/glycerol (3D) signals clearly

decline at higher temperatures, suggesting that conformational dynamics of mobile lipid head groups and FA segments are suppressed. The lipid spectral profiles do not change with temperature and from analysis of lipid peak intensities we exclude significant changes in lipid unsaturation or isomerization. The reduced lipid dynamics at high temperatures could be associated with a phase transition in the membrane. The INEPT temperature curves suggest that there is a mechanism (phase transition or other) that effectively protects the photosynthetic membranes against extreme membrane fluidity at high temperatures, unrelated to lipid saturation or isomerization, which would be of interest to further explore.

The temperature profiles of the thylakoid sample (figure 4) cannot directly be compared to the whole-cell sample, because of the increased sensitivity for INEPT detection in the thylakoid experiment due to higher MAS frequency that was used, and because of the limited temperature range over which the thylakoid preparations could be recorded without thermal damage. In the overlapping temperature range, the overall dynamic behavior is similar. the relative INEPT intensities of the lipid signals in the thylakoid spectrum in this work (4C) are higher than observed in the study in chapter 2 [21], where we concluded that the major lipid fraction did not display fast dynamics, and only a small fraction of lipids had mobile FA tails. In chapter 2 we also observed larger effect of lipid isomerization with temperature. Here we observe only small effect of isomerization and find that the majority of the lipids have very flexible end tails. A difference in sample conditions was that in the former study the water content of the rotor sample preparations was lower, which could have reduced the lipid conformational dynamics. In addition, the thylakoid preparations studied in chapter 2 were from different strains and had been stored at -80^{o}C before use, using glycerol as a cryo-protectant, whereas the thylakoid preparation in this study contained sucrose and was freshly prepared.

Conclusion

We demonstrate that ^{13}C NMR spectral editing can identify lipid, protein, sugar and cell wall constituents and resolve and quantify molecular dynamics of different cellular components, in particular lipid FA, in intact photosynthetic cells. Sample preparation typically involved growing a 50ml *Cr*. culture for 2-3 days and using 1,2-^{13}C acetate as a carbon source, which is very feasible both in terms of labor and label expenses. The presented spectra were each recorded with 64 scans, which typically takes about 10 minutes for scan accumulation.

However, we noticed that after rotor insertion, spectral changes occurred during MAS in the first 30-60 minutes, presumably due to slow sedimentation of cells on the rotor walls. Thus, the samples need to be spun for at least one hour in the rotor at the set spinning frequency before starting the measurements. MAS spinning did not break the cells at 5 kHz spinning frequency, which was checked afterward using an ordinary light microscope.

References

1. Betterle, N.; Ballottari, M.; Zorzan, S.; de Bianchi, S.; Cazzaniga, S.; Dall'osto, L.; Morosinotto, T.; Bassi, R., Light-induced Dissociation of an Antenna Hetero-oligomer Is Needed for Non-photochemical Quenching Induction. *Journal of biological chemistry* **2009,** *284* (22), 15255-15266.
2. Cruz, J.; Avenson, T.; Kanazawa, A.; Takizawa, K.; Edwards, G.; Kramer, D., Plasticity in light reactions of photosynthesis for energy production and photoprotection. *Journal of experimental botany* **2005,** *56* (411), 395-406.
3. Erickson, E.; Wakao, S.; Niyogi, K. K., Light stress and photoprotection in Chlamydomonas reinhardtii. *Plant J* **2015,** *82* (3), 449-65.
4. Tardy, F.; Havaux, M., Thylakoid membrane fluidity and thermostability during the operation of the xanthophyll cycle in higher-plant chloroplasts. *Biochimica et biophysica acta* **1997,** *1330* (2), 179-93.
5. Lambrev, P. H.; Nilkens, M.; Miloslavina, Y.; Jahns, P.; Holzwarth, A. R., Kinetic and Spectral Resolution of Multiple Nonphotochemical Quenching Components in Arabidopsis Leaves. *Plant Physiology* **2010,** *152* (3), 1611-1624.
6. Wlodarczyk, L. M.; Snellenburg, J. J.; Ihalainen, J. A.; van Grondelle, R.; van Stokkum, I. H.; Dekker, J. P., Functional Rearrangement of the Light-Harvesting Antenna upon State Transitions in a Green Alga. *Biophysical Journal* **2015,** *108* (2), 261-271.
7. Ünlü, C.; Drop, B.; Croce, R.; van Amerongen, H., State transitions in Chlamydomonas reinhardtii strongly modulate the functional size of photosystem II but not of photosystem I. *Proceedings of the National Academy of Sciences* **2014,** *111* (9), 3460-3465.
8. Amarnath, K.; Zaks, J.; Park, S. D.; Niyogi, K. K.; Fleming, G. R., Fluorescence lifetime snapshots reveal two rapidly reversible mechanisms of photoprotection in live cells of Chlamydomonas reinhardtii. *Proceedings of the National Academy of Sciences* **2012,** *109* (22), 8405-8410.
9. Kóta, Z.; Horváth, L. I.; Droppa, M.; Horváth, G.; Farkas, T.; Páli, T., Protein assembly and heat stability in developing thylakoid membranes during greening. *Proceedings of the National Academy of Sciences of the United States of America* **2002,** *99* (19), 12149-12154.
10. Szalontai, B.; Nishiyama, Y.; Gombos, Z.; Murata, N., Membrane dynamics as seen by Fourier transform infrared spectroscopy in a cyanobacterium, Synechocystis PCC 6803: The effects of lipid unsaturation and the protein-to-lipid ratio. *Biochimica et Biophysica Acta (BBA) - Biomembranes* **2000,** *1509* (1–2), 409-419.
11. Ruban, A. V.; Berera, R.; Ilioaia, C.; van Stokkum, I. H. M.; Kennis, J. T. M.; Pascal, A. A.; van Amerongen, H.; Robert, B.; Horton, P.; van Grondelle, R., Identification of a mechanism of photoprotective energy dissipation in higher plants. *Nature* **2007,** *450* (7169), 575-578.

12. Mullineaux, C. W.; Sarcina, M., Probing the dynamics of photosynthetic membranes with fluorescence recovery after photobleaching. *Trends in Plant Science 7* (6), 237-240.
13. Krumova, S. B.; Koehorst, R. B. M.; Bóta, A.; Páli, T.; van Hoek, A.; Garab, G.; van Amerongen, H., Temperature dependence of the lipid packing in thylakoid membranes studied by time- and spectrally resolved fluorescence of Merocyanine 540. *Biochimica et Biophysica Acta (BBA) - Biomembranes* **2008,** *1778* (12), 2823-2833.
14. Krumova, S. B.; Dijkema, C.; de Waard, P.; Van As, H.; Garab, G.; van Amerongen, H., Phase behavior of phosphatidylglycerol in spinach thylakoid membranes as revealed by 31P-NMR. *Biochimica et Biophysica Acta (BBA) - Biomembranes* **2008,** *1778* (4), 997-1003.
15. van Eerden, F. J.; de Jong, D. H.; de Vries, A. H.; Wassenaar, T. A.; Marrink, S. J., Characterization of thylakoid lipid membranes from cyanobacteria and higher plants by molecular dynamics simulations. *Biochimica et Biophysica Acta (BBA) - Biomembranes* **2015,** *1848* (6), 1319-1330.
16. van Eerden, F. J.; van den Berg, T.; Frederix, P. W. J. M.; de Jong, D. H.; Periole, X.; Marrink, S. J., Molecular Dynamics of Photosystem II Embedded in the Thylakoid Membrane. *The Journal of Physical Chemistry B* **2017,** *121* (15), 3237-3249.
17. Ogata, K.; Yuki, T.; Hatakeyama, M.; Uchida, W.; Nakamura, S., All-Atom Molecular Dynamics Simulation of Photosystem II Embedded in Thylakoid Membrane. *Journal of the American Chemical Society* **2013,** *135* (42), 15670-15673.
18. Arnold, A. A.; Genard, B.; Zito, F.; Tremblay, R.; Warschawski, D. E.; Marcotte, I., Identification of lipid and saccharide constituents of whole microalgal cells by (1)(3)C solid-state NMR. *Biochim Biophys Acta* **2015,** *1848* (1 Pt B), 369-77.
19. Pham, Q. D.; Topgaard, D.; Sparr, E., Tracking solvents in the skin through atomically resolved measurements of molecular mobility in intact stratum corneum. *Proceedings of the National Academy of Sciences* **2017,** *114* (2), E112-E121.
20. Nowacka, A.; Mohr, P. C.; Norrman, J.; Martin, R. W.; Topgaard, D., Polarization Transfer Solid-State NMR for Studying Surfactant Phase Behavior. *Langmuir* **2010,** *26* (22), 16848-16856.
21. Azadi Chegeni, F.; Perin, G.; Sai Sankar Gupta, K. B.; Simionato, D.; Morosinotto, T.; Pandit, A., Protein and lipid dynamics in photosynthetic thylakoid membranes investigated by in-situ solid-state NMR. *Biochimica et Biophysica Acta (BBA) - Bioenergetics* **2016,** *1857* (12), 1849-1859.
22. Porra, R.J.; Thompson, w. A.; Kriedemann, P. E, Determination of accurate extinction coefficients and simultaneous equations for assaying chlorophylls a and b extracted with four different solvents: verification of the concentration of chlorophyll standards by atomic absorption spectroscopy *Biochimica et biophysica acta* **1989,** *975*, 384-394.
23. Lawson, C. L.; Hanson, R. J., *Solving least squares problems*. SIAM: 1995; Vol. 15.
24. Bro, R.; De Jong, S., A fast non-negativity-constrained least squares algorithm. *Journal of Chemometrics* **1997,** *11* (5), 393-401.
25. Chua, N. H.; Bennoun, P., Thylakoid membrane polypeptides of Chlamydomonas reinhardtii: wild-type and mutant strains deficient in photosystem II reaction center. *Proceedings of the National Academy of Sciences of the United States of America* **1975,** *72* (6), 2175-2179.
26. Guan, X.; Stark, R. E., A general protocol for temperature calibration of MAS NMR probes at arbitrary spinning speeds. *Solid State Nucl Magn Reson* **2010,** *38* (2-3), 74-6.
27. Nowacka, A.; Mohr, P. C.; Norrman, J.; Martin, R. W.; Topgaard, D., Polarization transfer solid-state NMR for studying surfactant phase behavior. *Langmuir* **2010,** *26* (22), 16848-56.

28. Nowacka, A.; Bongartz, N. A.; Ollila, O. H. S.; Nylander, T.; Topgaard, D., Signal intensities in 1H–13C CP and INEPT MAS NMR of liquid crystals. *Journal of Magnetic Resonance* **2013,** *230*, 165-175.
29. Castro, V.; Dvinskikh, S. V.; Widmalm, G.; Sandström, D.; Maliniak, A., NMR studies of membranes composed of glycolipids and phospholipids. *Biochimica et Biophysica Acta (BBA) - Biomembranes* **2007,** *1768* (10), 2432-2437.
30. Coddington, J. M.; Johns, S. R.; Leslie, D. R.; Willing, R. I.; Bishop, D. G., 13C Nuclear magnetic resonance studies of the composition and fluidity of several chloroplast monogalactosyldiacylglycerols. *Biochimica et Biophysica Acta (BBA) - Lipids and Lipid Metabolism* **1981,** *663* (3), 653-660.
31. Moss, G. P., Carbon-13 NMR Spectra of Carotenoids. In *Pure and Applied Chemistry*, 1976; Vol. 47, p 97.
32. Lötjönen, S.; Hynninen, P. H., Carbon-13 NMR spectra of chlorophyll a, chlorophyll a′, pyrochlorophyll a and the corresponding pheophytins. *Organic Magnetic Resonance* **1983,** *21* (12), 757-765.
33. Markley, J. L.; Ulrich, E. L.; Berman, H. M.; Henrick, K.; Nakamura, H.; Akutsu, H., BioMagResBank (BMRB) as a partner in the Worldwide Protein Data Bank (wwPDB): new policies affecting biomolecular NMR depositions. *J Biomol NMR* **2008,** *40* (3), 153-5.
34. de Souza, L. M.; Iacomini, M.; Gorin, P. A.; Sari, R. S.; Haddad, M. A.; Sassaki, G. L., Glyco- and sphingophosphonolipids from the medusa Phyllorhiza punctata: NMR and ESI-MS/MS fingerprints. *Chem Phys Lipids* **2007,** *145* (2), 85-96.